INT. J. NUM. METH. HEAT FLUID FLOW, VOL. 5, 829–837 (1995)

CONVECTIVE HEAT TRANSFER IN AXISYMMETRIC POROUS BODIES

RAJESH RAJAMANI, C. SRINIVAS, P. NITHIARASU AND K. N. SEETHARAMU

Department of Mechanical Engineering, Indian Institute of Technology, Madras-600036, India

ABSTRACT

A finite element method employing Galerkin's approach is developed to analyze free convection heat transfer in axisymmetric fluid saturated porous bodies. The method is used to study the effect of aspect ratio and radius ratio on Nusselt number in the case of a proous cylindrical annulus. Two cases of isothermal and convective boundary conditions are considered. The Nusselt number is always found to increase with radius ratio and Rayleigh number. It exhibits a maximum when the aspect ratio is around unity; maximum shifts towards lesser aspect ratios as Rayleigh number increases. Results are compared with those in the literature, wherever available, and the agreement is found to be good.

KEY WORDS Heat transfer Porous bodies Cylindrical annulus

NOMENCLATURE

A	aspect ratio	r_i, r_o	inner and outer radius of the cylinder
ψ	streamline function	T	temperature
ε	porosity of the medium	μ	viscosity
$\overline{R}$	average radius of an element	ν	kinamatic viscosity
u, v, w	velocity in r, θ, and z directions	ρ	density
β	thermal expansion coefficient	α	thermal diffusivity
K_m	thermal conductivity of the saturated medium	K	permeability
N_1, N_2, N_3	shape functions for the triangular element	p	pressure

INTRODUCTION

Vertical porous enclosures with cylindrical geometry are encountered in many situations. Insulated pipe lines, cryogenic containers, insulation of high temperature gas cooled reactor vessels are some examples involving porous bodies of an axisymmetric geometry.

A knowledge of the variation of heat transfer with aspect ratio would be very useful in determining optimum insulation thickness. Nath and Satyamurthy[1] used a finite difference method to evaluate the variation of Nusselt number with aspect ratio, radius ratio and Rayleigh number. They provide results in the range $50 \leqslant Ra \leqslant 500$; $0.2 \leqslant A \leqslant 8$ and $0.25 \leqslant R^* \leqslant 8$. Little other attention has been paid in the literature to study the dependence of Nusselt number on the above parameters. Prasad and Kullacki[2] carried out a study of curvature effects on temperature and velocity fields in a vertical porous annulus. They considered a wide range of Rayleigh numbers, Ra up to 10,000.

0961–5539/95/090829–10$2.00

Received June 1993
Revised January 1995

Several authors have studied the limitations of Darcy's law. Cheng[3] in his review article mentioned that the Darcy's law is valid when the Darcy number based on the height is less than 10^{-3}. Tong and Subramanian[5] undertook a boundary layer analysis in vertical porous enclosures. They determined the validity of Darcy's law in terms of E ($Ra\ Da/A$). They indicated the limitation as $E<10^{-4}$. Lauriat and Prasad[7] examined relative importance of inertia and viscous forces on natural convection in porous media. They found, from their combined Brinkman and Forchheimer model, that the Darcy model is limited to Ra^* ($\lambda\ Ra(Da)<10^2$ for $\wedge Da=10^{-4}$ and $A=1$ where $\wedge$ is the viscosity ratio and λ is the conductivity ratio.

The present work uses Darcy's flow equations with continuity and energy to model the convective heat transfer in fluid saturated axisymmetric porous bodies. Free convection in a vertical cylindrical annulus is studied using the method and heat transfer results are obtained in the range $50\leqslant Ra\leqslant 200$; $0.2\leqslant A\leqslant 8$ and $0.1\leqslant R^*\leqslant 8$. The case of an inner cold isothermal wall and a hot outer wall with the two horizontal insulated walls is studied and the Nusselt number values are compared with published results[1]. The agreement was found to be good.

Next, the case of a hot isothermal inner wall with a convection boundary condition on the outer wall is considered. With an aspect ratio of unity, heat transfer results at different radius ratios are obtained.

FINITE ELEMENT FORMULATION

A cylindrical, saturated porous annulus of inner radius r_i and outer radius r_o is shown in the *Figure 1*. The coordinate system is also shown. Since the body is axysmmetric, two coordinates r and z are sufficient to describe the system completely.

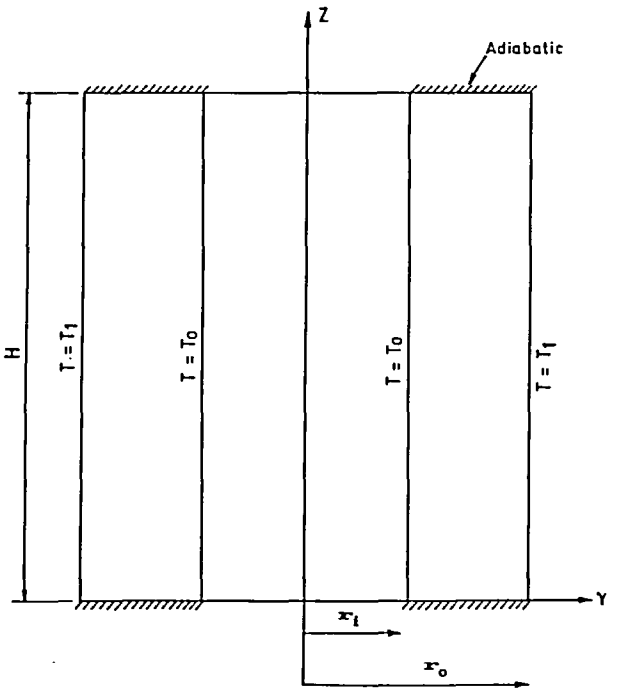

Figure 1 Coordinate system and geometry

We assume that,

(i) The porous medium considered is saturated by a fluid.
(ii) The porous medium is homogeneous and isotropic.
(iii) Fluid properties are constant except density variation which produces a buoyancy force.
(iv) The fluid and porous medium is everywhere in local thermodynamic equilibrium.
(v) Additional viscous and inertial terms are, for low Darcy numbers, neglected because of their small magnitudes compared to other terms.
(vi) Dispersion effects are neglected.

Under these assumptions, the governing equations in cylindrical coordinates are written as:

Continuity equation:

$$\frac{\partial(ru)}{\partial r}+\frac{\partial(rw)}{\partial z}=0 \tag{1}$$

Darcy's law in the r direction:

$$u=-\frac{\mathrm{K}}{\mu}\frac{\partial p}{\partial r} \tag{2}$$

Darcy's law in z direction:

$$w=-\frac{\mathrm{K}}{\mu}\left(\frac{\partial p}{\partial z}-\rho g\right) \tag{3}$$

Energy equation:

$$u\frac{\partial T}{\partial r}+w\frac{\partial T}{\partial z}=\alpha\left(\frac{1}{r}\frac{\partial}{\partial r}\left(r\frac{\partial T}{\partial r}\right)+\frac{\partial^2 T}{\partial z^2}\right) \tag{4}$$

Equation of state:

$$\rho=\rho_\infty(1-\beta(T-T_\infty)) \tag{5}$$

We introduce the stream function ψ defined by,

$$u=--\frac{1}{r}\frac{\partial\psi}{\partial z} \tag{6}$$

$$w=\frac{1}{r}\frac{\partial\psi}{\partial r} \tag{7}$$

The continuity equation is automatically satisfied by the introduction of ψ. One governing equation is thus eliminated.

Eliminating the variable p from (2) and (3) and incorporating ψ we obtain,

$$\frac{\mu}{K}\frac{1}{r}\left(\frac{\partial^2\psi}{\partial r^2}+\frac{\partial^2\psi}{\partial z^2}\right)+\frac{1}{r^2}\frac{\mu}{K}\frac{\partial\psi}{\partial r}=\rho_\infty\beta g\frac{\partial T}{\partial r} \tag{8}$$

Using $\nu=\mu/\rho$, we obtain,

$$\frac{\partial^2\psi}{\partial z^2}+\frac{1}{r}\frac{\partial}{\partial r}\left(r\frac{\partial\psi}{\partial r}\right)=r\frac{Kg\beta}{\nu}\frac{\partial T}{\partial r} \tag{9}$$

Substituting u and w in terms of ψ in (4), we obtain,

$$\alpha\left(\frac{1}{r}\frac{\partial}{\partial r}\left(r\frac{\partial T}{\partial r}\right)\right)=-\frac{1}{r}\frac{\partial\psi}{\partial z}\frac{\partial T}{\partial r}+\frac{1}{r}\frac{\partial\psi}{\partial r}\frac{\partial T}{\partial z} \tag{10}$$

Equations (9) and (10) are the two governing equations to be formulated into finite element matrix equations. Each equation has both the variables ψ and T, we thus have two coupled equations which have to be solved simultaneously.

The simplex 3 noded triangular element is used for the analysis. The variation of temperature T and ψ inside the element are given by,

$$T=N_1T_1+N_2T_2+N_3T_3 \\ =[N]\{T\} \tag{11}$$

$$\psi=N_1\psi_1+N_2\psi_2+N_3\psi_3 \\ =[N]\{\psi\} \tag{12}$$

where N_1, N_2, and N_3 are the shape functions given by,

$$N_i=\frac{a_i+b_ir+c_iz}{2A} \qquad i=1, 2, 3 \tag{13}$$

Using Gallerkin's method, (9) becomes,

$$\int_V N^T\left(\frac{\partial^2\psi}{\partial z^2}+\frac{1}{r}\frac{\partial}{\partial r}\left(r\frac{\partial\psi}{\partial r}\right)-\frac{Kg\beta}{\nu}r\frac{\partial T}{\partial r}\right)dV=0 \tag{14}$$

where $dV=2\pi r\,dr\,dz$ for axisymmetric geometries. Integration of first two terms gives,

$$\left(\frac{2\pi\bar{R}}{4A}\begin{bmatrix} b_1^2 & b_1b_2 & b_1b_3 \\ b_1b_2 & b_2^2 & b_2b_3 \\ b_1b_3 & b_2b_3 & b_3^2 \end{bmatrix}+\frac{2\pi\bar{R}}{4A}\begin{bmatrix} c_1^2 & c_1c_2 & c_1c_3 \\ c_1c_2 & c_2^2 & c_2c_3 \\ c_1c_3 & c_2c_3 & c_3^2 \end{bmatrix}\right) \tag{15}$$

The third term in the parenthesis is,

$$\int N^T\left(\frac{Kg\beta}{\nu}r\frac{\partial T}{\partial r}\right)2\pi r\,dr\,dz=2\pi\bar{R}^2\frac{Kg\beta}{6\nu}\begin{Bmatrix} b_1T_1+b_2T_2+b_3T_3 \\ b_1T_1+b_2T_2+b_3T_3 \\ b_1T_1+b_2T_2+b_3T_3 \end{Bmatrix} \tag{16}$$

Similarly, use of Galerkin's method for (10) yields,

$$\int N^T\left[\alpha\frac{1}{r}\frac{\partial}{\partial r}\left(r\frac{\partial T}{\partial r}\right)+\alpha\frac{\partial^2T}{\partial z^2}+\frac{1}{r}\frac{\partial\psi}{\partial z}\frac{\partial T}{\partial r}-\frac{1}{r}\frac{\partial\psi}{\partial r}\frac{\partial T}{\partial z}\right]2\pi r\,dr\,dz=0 \tag{17}$$

Integrating, the first two terms in the parenthesis become,

$$\frac{2\pi\bar{R}\alpha}{4A}\begin{bmatrix} b_1^2 & b_1b_2 & b_1b_3 \\ b_1b_2 & b_2^2 & b_2b_3 \\ b_1b_3 & b_2b_3 & b_3^2 \end{bmatrix}+\frac{2\pi\bar{R}\alpha}{4A}\begin{bmatrix} c_1^2 & c_1c_2 & c_1c_3 \\ c_1c_2 & c_2^2 & c_2c_3 \\ c_1c_3 & c_2c_3 & c_3^2 \end{bmatrix} \\ +\frac{2\pi hL_{jk}}{12}\begin{bmatrix} 0 & 0 & 0 \\ 0 & 3R_j+R_k & R_j+R_k \\ 0 & R_j+R_k & R_j+3R_k \end{bmatrix}-\frac{2\pi hL_{jk}T_\infty}{6}\begin{Bmatrix} 0 \\ 2R_j+R_k \\ R_j+2R_k \end{Bmatrix} \tag{18}$$

where jk is the side along which the convective boundary condition exists.

$$\int_V N^T \frac{1}{r}\frac{\partial \psi}{\partial z}\frac{\partial T}{\partial r}\,dV = \frac{2\pi}{12A}\begin{bmatrix} c_1\psi_1+c_2\psi_2+c_3\psi_3 \\ c_1\psi_1+c_2\psi_2+c_3\psi_3 \\ c_1\psi_1+c_2\psi_2+c_3\psi_3 \end{bmatrix}[b_1\ b_2\ b_3]\begin{Bmatrix} T_1 \\ T_2 \\ T_3 \end{Bmatrix} \tag{19}$$

$$\int_V N^T \frac{1}{r}\frac{\partial \psi}{\partial r}\frac{\partial T}{\partial z}\,dV = \frac{2\pi}{12A}\begin{bmatrix} b_1\psi_1+b_2\psi_2+b_3\psi_3 \\ b_1\psi_1+b_2\psi_2+b_3\psi_3 \\ b_1\psi_1+b_2\psi_2+b_3\psi_3 \end{bmatrix}[c_1\ c_2\ c_3]\begin{Bmatrix} T_1 \\ T_2 \\ T_3 \end{Bmatrix} \tag{20}$$

Equations (15) through (20) yield two simultaneous matrix equations for an element. These matrix equations are assembled to obtain the total matrix equation for the domain. Initially the value of ψ is taken to be zero for the first iteration. The values of $\{T\}$ obtained by solving the first set of equations are then used to solve the second set of global matrix equations. These values of $\{\psi\}$ are then used for the next iteration in the calculation of $\{T\}$. The two equations are thus solved by iteration. For the solutions to converge it is necessary that a fine mesh is used. Convergence is obtained by maintaining the error limit to 10^{-5}. The values of $\{\psi\}$ at the wall are forced to zero (since $u=0$ at $x=0$). The temperature at the wall nodes are also incorporated.

Convergence is more difficult for the axisymmetric case than for simple two dimensional one[8]. For high Rayleigh numbers convergence becomes easy for very fine meshes.

RESULTS AND DISCUSSION

Consider the cylindrical porous annulus of *Figure 1*. Let the inner wall of radius r_i be isothermal at a temperature T_o and the outer wall radius r_o be at $T_1 > T_o$. The two horizontal walls are adiabatic. One half of the section in *Figure 1* is sufficient for the analysis. The rectangular region of length H and breadth $(r_o - r_i)$ is discretized into a finite element mesh. For larger Rayleigh numbers a finer mesh is required.

The Rayleigh number in the present case is defined as,

$$Ra = \frac{Kg\beta(T_1 - T_o)L}{\alpha\nu} \tag{21}$$

where $L = r_o - r_i$.

The boundary conditions of $u=0$ at $r=r_i$ and $r=r_o$ and $w=0$ at $z=0$ and $z=H$ are incorporated by forcing ψ to be zero on all four boundaries. The temperature on the two vertical walls are forced to be T_o and T_i.

Solution of the two finite equations by iteration, as described earlier, yields steady state temperature at all nodes.

The mean Nusselt number at the cold wall is calculated using the equation

$$\overline{Nu} = \frac{-\int K_m \frac{\partial T}{\partial r}\,dz}{K_m \Delta T \frac{H}{L}} \tag{22}$$

Curve fitting is used for the calculation of the derivative at each wall node.

Aspect ratio for the cylinder, A, is defined as $A = H/L$ and radius ratio as $R^* = (r_o - r_i)/r_i$.

Nusselt number values for $Ra = 100$ and $R^* = 1$ are compared with the results available in both References 1 and 2. The comparison is shown in *Table 1*.

Values obtained with finer discretization differed only marginally from the values in the table.

Table 1 Comparison of Nu results

Aspect ratio	Ref [1]	Ref [2]	Present calculation
3	3.81	3.70	3.868
5	3.03	3.00	3.025
8	2.45	2.35	2.403

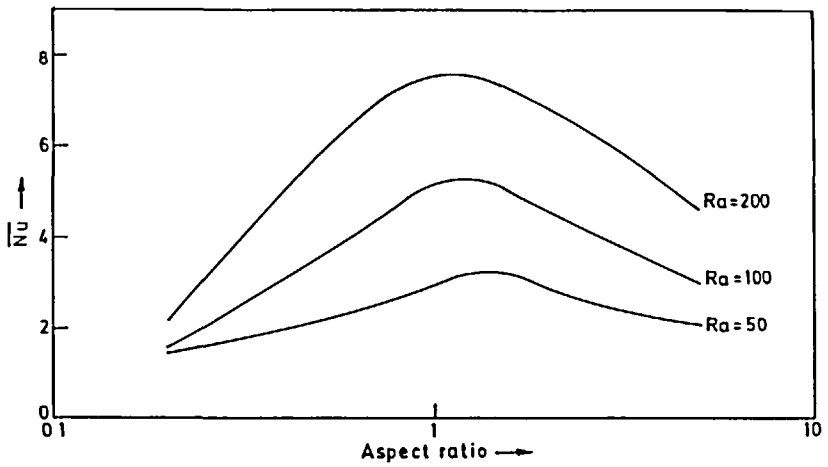

Figure 2 Nusselt Number vs Aspect Ratio

Table 2 Variation of Nusselt number with radius ratio

R^*	$A=0.6$			$A=5$		
	$Ra=50$	$Ra=100$	$Ra=200$	$Ra=50$	$Ra=100$	$Ra=200$
0.25	1.791	3.073	5.108	1.619	2.349	3.694
1	2.344	3.985	6.41	2.105	3.025	4.63
4	4.016	6.342	8.915	3.636	3.636	6.73
8	5.466	8.140	9.89	5.000	6.615	7.774

Variation of Nusselt number with aspect ratio

The variation of Nusselt number with aspect ratio for a radius ratio of one is shown in the *Figure 2*. Curves for $Ra=50$, 100 and 200 are shown. It is seen that each curve reaches a maxima for an aspect ratio around unity. The maxima shifts towards lower aspect ratios for higher Rayleigh numbers.

Variation of Nusselt number with radius ratio

The variation of Nusselt number with radius ratio for the two aspect ratios of 0.6 and 5 is shown in the *Table 2*.

It is seen that for a given Ra and aspect ratio, Nusselt number always increases with R^*. The maximum values of Nusselt number for different R^* were calculated using an aspect ratio of unity.

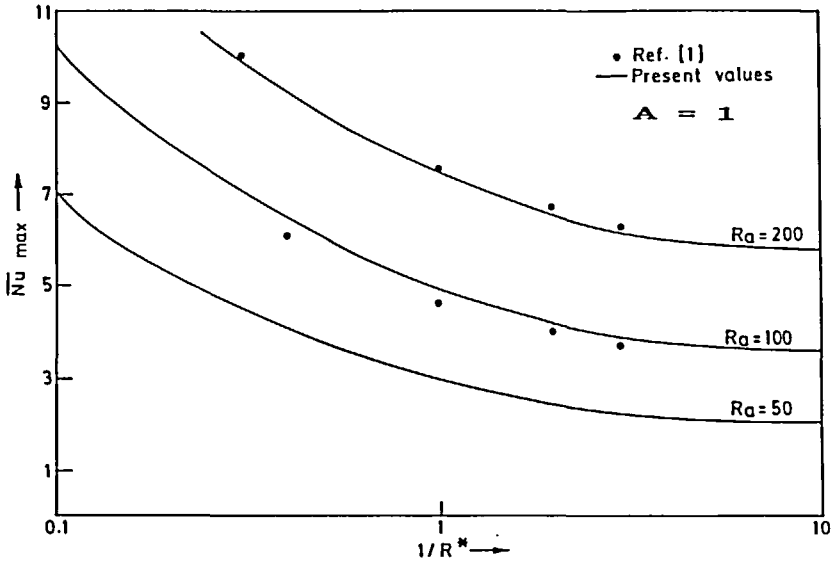

Figure 3 Nusselt Number vs 1/RADIUS Ratio

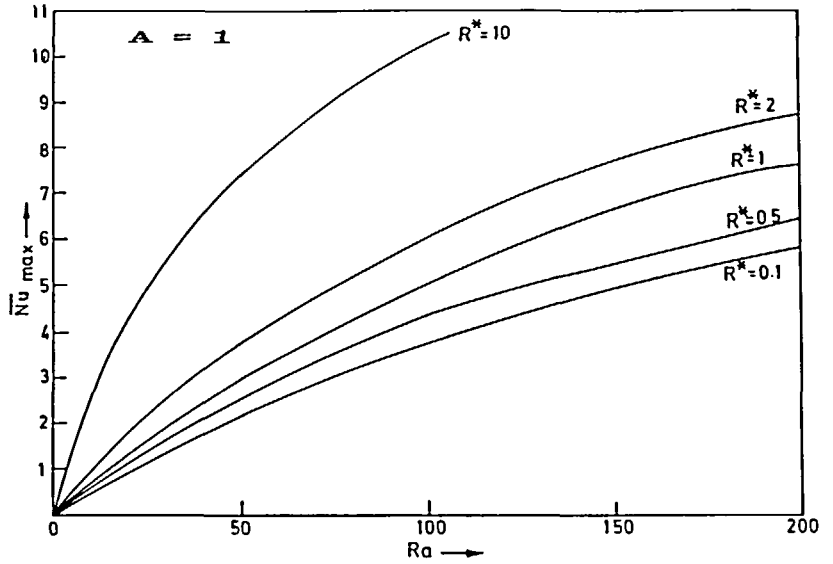

Figure 4 Nu_{max} vs Rayleigh Number

The variation of $\overline{Nu}_{max}$ with $1/R^*$ is shown in *Figure 3*. It is seen that $\overline{Nu}_{max}$ increases with R^* for every Rayleigh number. Curves for $Ra=50$, 100 and 200 are shown. as $R^* \to 0$, which is the case of plane slab, the curves approach asymptotic values of $\overline{Nu}_{max}$.

The variation of $\overline{Nu}_{max}$ with Rayleigh number is shown in *Figure 4* for different R^*. It is seen that $\overline{Nu}_{max}$ always increases with Rayleigh number. The increase is steep for lower Ra and becomes small for $Ra > 200$.

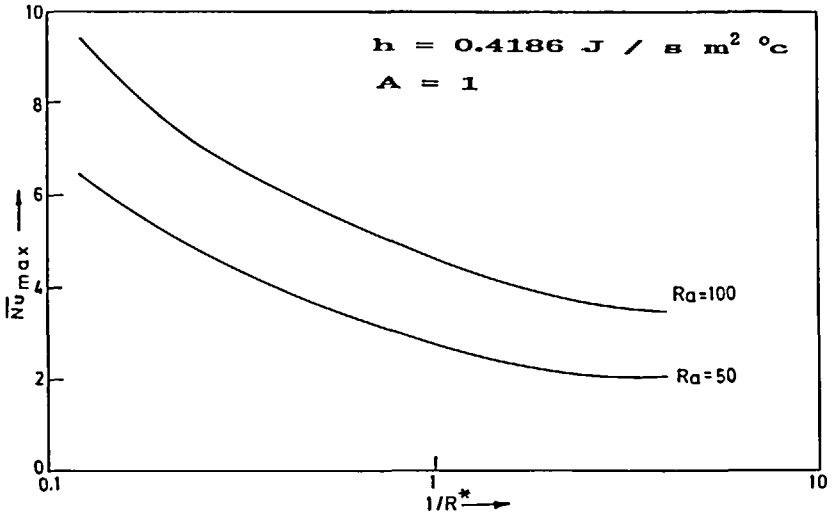

Figure 5 Nu_{max} vs 1/Radius Ratio

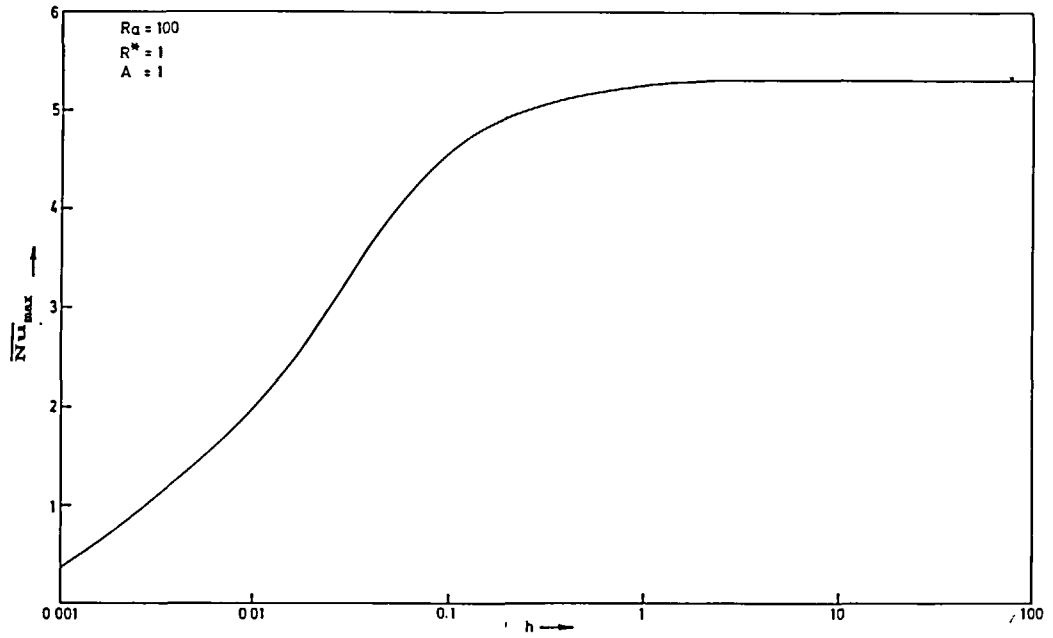

Figure 6 Variation of Nusselt Number with heat transfer coefficient

Many practical situations involve a porous cylindrical annulus with an inner hot surface and a convection boundary condition on the outer surface. This case is considered next with assumption that the inner wall is isothermal. *Figure 5* shows the variation of $\overline{Nu}_{max}$ with $1/R^*$ for this case. It is seen that the variation is similar to that for an isothermal outer wall. A heat transfer coefficient of $h = 0.4186$ J/s m^2 °C has been taken. The values of $\overline{Nu}_{max}$ are lower for

lower values of h. As h increased above 1, $\overline{Nu}_{max}$ reaches an asymptotic maximum. *Figure 6* gives the variation of $\overline{Nu}_{max}$ with h for $Ra = 100$ and $R^* = 1$.

CONCLUSIONS

A finite element model to analyze free convection heat transfer in vertical porous enclosures was developed. The case of a porous cylindrical annulus with an isothermal inner wall and outer wall with a convection boundary condition or an isothermal condition were considered. The variation of Nusselt number with aspect ratio, radius ratio and Rayleigh number are studied. Nusselt number always increases with radius ratio as well as Rayleigh number and attains a maximum for an aspect ratio around unity. Results have been compared with those available in literature and the agreement is found to be good.

REFERENCES

1 Nath, S. K. and Satyamurthy, V. V. Effect of aspect ratio and radius ratio on free convection heat transfer in a cylindrical annulus filled with porous media, *HMT C16-85, Proc. 8th Nat. Heat and Mass Transfer Conf. India*, 189–193 (1985)
2 Prasad, V. and Kulacki, F. A. Natural convection in a vertical porous annulus, *Int. J. Heat Mass Transfer*, **V27**, 207–219 (1984)
3 Cheng, P. Heat transfer in geothermal systems, *Adv. Heat Transfer*, **14**, 1–105 (1979)
4 Prasad, V. Numerical study of natural convection in a vertical porous annulus with constant heat flux on the inner wall. *Int. J. Heat Mass Transfer*, **V29**, 841–853 (1986)
5 Tong, T. W. and Subramanian, E. A boundary analysis for natural convection in vertical porous enclosures—use of Brinkman—extended Darcy model, *Int. J. Heat Mass Transfer*, **28**, 563–571 (1985)
6 Segerlind, L. J. *Applied Finite Element Method*, John Wiley and Sons (1982)
7 Lauriat, G. and Prasad, V. Non-Darcian effects on natural convection in a vertical porous enclosure, *Int. J. Heat Mass Transfer*, **V32**, 2135–2158 (1989)
8 Rajamani, R., Srinivas, C. and Seetharamu, K. N. Finite element analaysis of convective heat transfer in porous media, *Int. J. Num. Meth. in Fluids*, **VII**, 331–339 (1990)
9 Rajamani, R. FEM applications in analysis of free convection in porous media, B.Tech Thesis, Dept. of Mechanical Engineering, Indian Institute of Technology, Madras (1989)